Passive Vibration Damping Using Polymer Pads With Microchannel Arrays

ARTICLE *in* JOURNAL OF MICROELECTROMECHANICAL SYSTEMS · JUNE 2013

Impact Factor: 1.75 · DOI: 10.1109/JMEMS.2013.2241392

7 AUTHORS, INCLUDING:

Rishi Kant

Indian Institute of Technology Kanpur

11 PUBLICATIONS **9** CITATIONS

SEE PROFILE

Mohammed Asfer

Indian Institute of Technology Kanpur

6 PUBLICATIONS **6** CITATIONS

SEE PROFILE

Bishakh Bhattacharya

Indian Institute of Technology Kanpur

64 PUBLICATIONS **157** CITATIONS

SEE PROFILE

Shantanu Bhattacharya

Indian Institute of Technology Kanpur

46 PUBLICATIONS **490** CITATIONS

SEE PROFILE

Passive Vibration Damping Using Polymer Pads With Microchannel Arrays

Rajeev Kumar Singh, Rishi Kant, Shashank Shekhar Pandey, Mohammed Asfer, Bishakh Bhattacharya, Pradipta K. Panigrahi, and Shantanu Bhattacharya

***Abstract*—Passive vibration control using blocks of viscoelastic materials with macro- and microscopic inclusions has been widely investigated. Significant changes in the vibration response have been observed with such inclusions. We have found that their response changes much more significantly if thin microstructures and channels are carved within these materials and are filled with a high-viscosity fluid. In this paper, we report the passive response of a replicated array of oil-filled microchannels, structured within a block made up of polydimethylsiloxane. Constrained and unconstrained vibration-damping experiments are performed on this block, wherein its vibration suppression ability is detected by applying an excitation signal transversely at the geometric center of the lower face of the block. We observe an increase in the fundamental frequency due to change in stiffness of the block and an increase in damping ratio and loss factor owing to the development of a slip boundary condition between the oil and the microchannel walls causing frictional dissipation of the coupled energy. All vibration experiments have been performed using a single-point laser to ascertain the experimental behavior of the system. We have also modeled the vibration suppression characteristics of such systems both analytically and by using simulation tools [2011-0273]**

***Index Terms*—Aluminium plate, damper, damping ratio, fundamental frequency, loss factor, microchannel, polydimethylsiloxane (PDMS), vibration.**

I. Introduction

VIBRATION damping is essential in prolonging the lifecycle of machinery and structures, in reducing human discomfort, and in high-precision machining and can be performed by vibration reduction at the source, vibration isolation, system modification, active vibration control, energy harvesting, etc. [1]. Also, high-precision machines require very low vibration ambience to work properly. Vibrations may be linear or nonlinear. If all of the basic components of vibrating systems, like mass, damper, and spring, are working linearly, the resulting vibrations are known as linear, while if one or more of the vibrating systems work nonlinearly, then vibrations are said to be nonlinear. The choice of suitable material plays an important role in vibration isolation and system modification. For example, polymers are good candidates for vibration damping, and they work very efficiently near the glass transition temperature [2]. In viscoelastic polymers, the energy dissipation takes place as a result of friction between different chains of oligomers during their cyclic deformation. There are many viscoelastic polymers, such as polyurethanes, poly(vinyl acetate), acrylics, natural rubber, styrene-butadiene rubber, and polydimethylsiloxane (PDMS), used commonly for vibration suppression, depending on the temperature and frequency range of operation.

The distinguishing features of these polymers are their enormous resilience and high energy dissipation capacity, although their elastic modulus and damping capacity are highly sensitive to change in vibration frequency (i.e., the loading rate) and temperature [3]. A vibration isolator made up of such viscoelastic solids can be shaped either as an insert, which can be placed in a cavity anywhere within the structure or a laminate which is placed between external surfaces of the structure [4].

In the laminate configuration, vibration isolation can be achieved in a constrained mode in which the damping layer (PDMS in our case) is sandwiched between two metallic plates of equal thickness, with one acting as a supporting plate (host) and the other acting as a stiff constraining layer, resulting in shear deformation of the damping layer. In the other configuration, the laminate can be used in unconstrained mode, wherein the damping layer does not have the constraining aluminum layer and the vibration damping is primarily due to the extensional deformation of the damping layer [3]. The objective of an effective damping treatment is to add the viscoelastic material in a manner so that it can withstand the heaviest amount of cyclic deformation. The main reason of investigating the damping behavior as constrained and unconstrained cases is that, in the former, the dominant mechanism of vibration isolation is shear deformation and, in the later, it is through flexural bending. The theory of damped structures has been thoroughly investigated in recent years. Teng *et al.* [5] have performed detailed studies of the damping characteristics of viscoelastic laminates in both the constrained and unconstrained cases and have studied the effects of temperature, frequency, and dimensions

Manuscript received September 13, 2011; revised November 18, 2012; accepted January 1, 2013. Date of publication February 22, 2013; date of current version May 29, 2013. This work was supported in part by the Dean of Research and Development, Indian Institute of Technology, Kanpur, India, and in part by the Department of Biotechnology and National Program on Materials and Smart Structures, Government of India. Subject Editor C. Mastrangelo.

R. K. Singh, R. Kant, M. Asfer, P. K. Panigrahi, and S. Bhattacharya are with the Microsystems Fabrication Laboratory, Department of Mechanical Engineering, Indian Institute of Technology, Kanpur 208016, India (e-mail: rajeevme@iitk.ac.in; rishikt@iitk.ac.in; mdasfer@iitk.ac.in; panig@iitk.ac.in; bhattacs@iitk.ac.in).

S. S. Pandey is with the University of Utah, Salt Lake City, UT 84112 USA.

B. Bhattacharya is with the SMSS Laboratory, Department of Mechanical Engineering, Indian Institute of Technology, Kanpur 208016, India (e-mail: bishakh@iitk.ac.in).

Color versions of one or more of the figures in this paper are available online at http://ieeexplore.ieee.org.

Digital Object Identifier 10.1109/JMEMS.2013.2241392

of damped structures on vibration-damping characteristics. Kerwin *et al.* [6] developed a theory for flexural beams to study damping effects of viscoelastic material for constrained layer damping (CLD). Ross *et al.* [7] derived the loss factor in terms of energy dissipation for such viscoelastic materials. Rao *et al.* [8] examined unsymmetric sandwich beams and plates with cores made up of viscoelastic materials. Johnson *et al.* [9] briefly reviewed the techniques employed for design in passive damping for vibration control. The investigation also categorized viscoelastic materials as one of the most commonly used material for damping and discussed some of the design methods and testing/characterization of these materials for passive damping. Marcelin *et al.* [10] analyzed a beam constrained by a viscoelastic layer for optimal damping by covering several portions of the beam. Thus, one can tune the viscoelastic damper, making it efficient in a specified frequency range. However, such tuning is limited to a prespecified frequency band. Bhattacharya *et al.* [1] have worked on different active CLD strategies where an active layer placed on top of the constraining layer has been used to maximize shear deformation in the viscoelastic layer. This has shown a larger bandwidth and better tenability. Researchers have also investigated the influence of passive micro- and macroscale inclusions in viscoelastic composites on their vibration-damping properties. Patel *et al.* [11] have modeled the effect of microscale inclusions in polymers and have predicted that nanostructured viscoelastic inclusion can change significantly the loss factor of a matrix over a wide frequency band. Goel *et al.* [12] studied the effects of gold, silver, and platinum nanoparticles embedded in PDMS on vibration-damping properties and found out a change in the damping factor from 0.09 to 0.13 (1.4 times) in a frequency range of 1–9 Hz. They further observed a fall in the damping factor beyond this range of frequency. Kaully *et al.* [13] studied the microscale damping behavior of PDMS with calcium carbonate inclusions by varying the volume fraction of calcium carbonate and operational temperature. The optimum range of operational temperature was found as $-120- -35\,^{\circ}$C, and a loss factor variation of 0.01–0.19 (19 times) was observed for various volume fractions of the inclusion within this temperature range. Wang *et al.* [14] studied the damping behavior of shape memory alloys with graphite particulate inclusions present in macroscopic sizes and observed an increase in the internal friction (representing the loss factor) from 0.02 to 0.18 at an optimum operational temperature of 323 °C.

Although a lot of work has been done on viscoelastic laminates using them as damping layers (in both constrained and unconstrained modes) either directly or with various additives and inclusions, the impact of microstructuring of these laminates to vibration suppression remains by and large unexplored. In this paper, we have developed a novel viscoelastic laminate (made up of PDMS) slab by replicating microchannel arrays within the slab and then by filling them with viscous oil, followed by sealing the ends of this microchannel with PDMS. We have further found out the impact of this replication and filling on vibration damping. We have observed that both damping ratio and fundamental frequencies can be customized by appropriately microstructuring the viscoelastic layer. Unlike the methods cited earlier, the significance of this method lies in its ability to incorporate vibration suppression at room temperature and high frequency bandwidth. Also, this methodology is independent of any other constraint imposed by dispersion of phases, like clustering or change in size, which has been always prominent in the inclusion methods as illustrated earlier.

Fundamental mode frequency and damping ratio are obtained experimentally for the constrained and unconstrained configurations, and a mathematical model is developed for the unconstrained treatment case. This observation is of fundamental importance as this would open a new dimension of structuring of damping layers to achieve a desirable level of passive vibration control. We have also evaluated the behavior of the oil contained within these microchannel arrays and have found that a slip boundary condition gets created, owing to which there is a substantial frictional energy dissipation at the fluid structure interface. This explains the increase in damping ratio for the microstructured laminates.

A. Theory

A mathematical model is proposed to analyze the unconstrained configuration of the microstructured laminate. The PDMS slab is fixed on the aluminum base plate (damper assembly) to avoid any relative motion between the two, particularly, while applying the excitation signal or impact. In the damper assembly, as the PDMS slab is pasted by a thin layer of liquid PDMS material, there is some shrinkage of the adhesive layer (1%–3% for the PDMS layer) [15] on heat curing, which causes the PDMS slab to have a residual compressive load. In the unconstrained case, this load emanates from the bottom face, thus emerging a trapezoidal structure, and in the constrained case, it emanates from both faces [bitrapezoidal structure; Fig. 1(a) and (b)].

Our analysis consists of laminates from one to four layers of microchannel arrays (rowwise) with 20 microchannels in each row. We have tried to find out the analytical solution of the fundamental frequency using the indicated geometries, with negligible adhesive layer thickness between the laminate and the aluminum base plate. The analytical model constructed here is that of a composite damper, with one phase as the PDMS matrix and the other phase as the silicone-oil-filled microchannels. Since microchannels have a large surface-area-to-volume ratio, their mechanical properties can be well estimated using the whole surface area of the channel instead of the cross-sectional area. The total surface area "A_m" occupied by these microchannels is

$$A_m = n \times 2\pi r(r + l) \tag{1}$$

where n is the total number of microchannels, r is the channel radius, and l is the length of the channels. Let us assume the transverse cross-sectional area of the whole PDMS slab and aluminum plate to be "A_s" and "A_l," respectively. In case of the microchannels filled with silicone oil, the entire surface of the channels is the source of dissipating vibrational energy because of the shear between the oil and the channel surface, and thus, the total surface available is very critical to vibration damping or frequency change. Therefore, total area of the composite

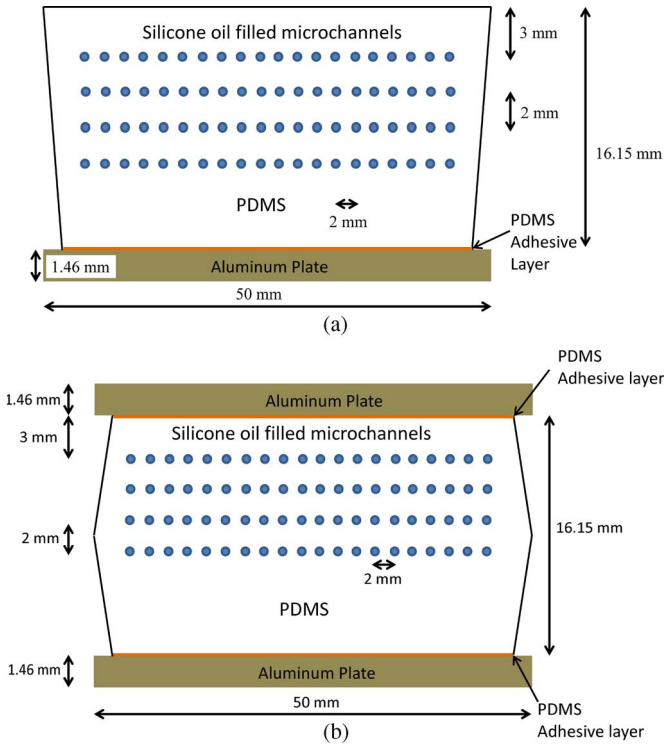

Fig. 1. (a) Trapezoidal shape of microvibration damper in unconstrained treatment. (b) Bitrapezoidal shape of microvibration damper in constrained treatment.

damper (A_{total}) is calculated by considering a contribution of the whole surface of an array of microchannels instead of the cross-sectional area. Thus,

$$A_{\text{total}} = A_m + A_s + A_l. \tag{2}$$

The area fraction occupied by the microchannel array is

$$A_{f_{mc}} = \frac{A_m}{A_{\text{total}}}. \tag{3}$$

The area fraction of the PDMS layer is

$$A_{f_{\text{PDMS}}} = \frac{A_s}{A_{\text{total}}}. \tag{4}$$

The area fraction of the aluminum plate is

$$A_{f_{\text{al}}} = \frac{A_l}{A_{\text{total}}}. \tag{5}$$

The density of the composite damper is calculated by using the rule of mixture as [16]

$$\rho = \rho_m A_{f_{mc}} + \rho_{\text{PDMS}} A_{f_{\text{PDMS}}} + \rho_{\text{al}} A_{f_{\text{al}}} \tag{6}$$

where ρ_{al}, ρ_{PDMS}, and ρ_m are the densities of aluminum, PDMS, and the material within the microchannels, which, in our case, is silicone oil.

According to classical theory for the free vibrations of rectangular thin plates, the governing equation for free vibration may be expressed as

$$D\nabla^4 w + \rho \frac{\partial^2 w}{\partial t^2} = 0 \tag{7}$$

where w is the transverse deflection of the plate, ∇^2 is the biharmonic differential operator (i.e., $\nabla^4 = \nabla^2\nabla^2$, $\nabla^2 = \partial^2/\partial x^2 + \partial^2/\partial y^2$ in rectangular coordinates), $D = Eh^3/12(1-v^2)$ is the flexural rigidity, E is the Young's modulus, h is plate thickness, v is the Poisson's ratio, ρ is mass density per unit area of plate surface, and t is time.

The boundary conditions for an edge parallel to the y-axis of the aforementioned equation for a clamped edge are

$$w = \frac{\partial w}{\partial x} = 0 \tag{8}$$

and for a free edge are

$$\frac{\partial^2 w}{\partial x^2} + v\frac{\partial^2 w}{\partial y^2} = \frac{\partial^3 w}{\partial x^3} + (2-v)\frac{\partial^3 w}{\partial x \partial y^2} = 0. \tag{9}$$

In order to solve (7), the Rayleigh–Ritz method can be used, wherein a function $W(x, y)$ is defined as

$$W(x,y) = \sum_{p,q} A_{pq} X_p(x) Y_q(y) \tag{10}$$

where X_p and Y_q are normalized eigenfunctions exactly satisfying the equation of motion of a freely vibrating uniform beam, and also, these satisfy the clamped, simply supported, or free-edge conditions at the ends of the beam. A_{pq} is the amplitude of $W(x, y)$ which can be used as a trial function for the solution of (7). The coefficients are determined by the Ritz method, with a view of minimizing an energy function to get the best approximation of the equation of motion (7). Clamped boundary conditions are exactly satisfied by the use of the beam functions, making the solution of (7) accurate, whereas for the clamped–free–clamped–free (C-F-C-F) case, four symmetry classes of modes exist, making the solution approximate. The procedure then reduces to yielding four ninth-order eigenvalue determinants on the right side of (10). Expanding the determinant and collecting terms yields a characteristic equation. We obtain a nondimensional frequency parameter λ from this characteristic equation, which is defined in the following:

$$\lambda = \omega a^2 \sqrt{\rho'/D} \tag{11}$$

where ω, a, D, and ρ' are the angular frequency of vibration of the plate, length, flexural rigidity, and density of the damper which possesses free vibrations analogous to the rectangular plate. The length-to-width ratio of the microvibration dampers is $a/b = 1.22 \approx 1.5$.

The calculated nondimensional frequency parameter λ for a C-F-C-F case for a length-to-width ratio of 1.5 is given as 22.272 [17]. The density of the microvibration damper in kilograms per square meter is defined as $\rho' = \rho \cdot a$, where a is length of the damper between fixed ends.

The λ parameter in (11) corresponds to a thin plate of a single material. In order to calculate the fundamental mode frequency of the microvibration damper laminates using (11), the twin laminate structure of the PDMS slab and aluminum plate needs to be reduced to an equivalent structure made up of aluminum using [18]

$$t' = \frac{E}{E'} t \tag{12}$$

where t' and t are the thicknesses of the equivalent aluminum layer and PDMS layer and E' and E are the Young's modulus of aluminum and PDMS, respectively. It is clear that the equivalent aluminum thickness of the PDMS slab should come much lesser, thus approximating the thin rectangular plate model described previously. A reverse conversion into an all PDMS equivalent would have a very high thickness which may not be solved using the thin-plate free-vibration equation.

The overall thickness of the microdamper assembly is given by $h=t'+t''$, where t'' and h are the thickness of the aluminum plate and the equivalent thickness of the damper assembly, henceforth referred to as "laminate equivalent." The flexural rigidity of the laminate equivalent is $D=Eh^3/12(1-v^2)$ [15], where E and v are the Young's modulus and Poisson's ratio of aluminum, respectively. Furthermore, the fundamental mode frequency f of the microvibration damper is given by $\omega=2\pi f$.

The measurement of damping characteristics is carried out using two general methods as described in the following discussion.

1) Logarithmic Decrement Method: When a single degree of freedom oscillatory system with viscous damping is excited by an impulse input, its response takes the form of a time decay. The logarithmic decay δ [2] is given by

$$\delta = \frac{1}{r}\ln\left(\frac{A_i}{A_{i+r}}\right) \tag{13}$$

where A_i and A_{i+r} denote first peak point and peak point r cycles later in the time decay, respectively. This method then yields the damping ratio, which is a dimensionless quantity that is used to measure the decay of vibration in a system. The damping ratio ζ is expressed as

$$\zeta = \frac{1}{\sqrt{1+\left(\frac{2\pi}{\delta}\right)^2}}. \tag{14}$$

2) Half-Power Bandwidth Method: It is a frequency response method. Bandwidth is defined as the width of the frequency response magnitude curve $(\Delta\omega.)$ when the magnitude is $1/\sqrt{2}$ times the peak value of the displacement amplitude. This also corresponds to the half-power point. The damping characteristic can then be estimated by calculating the loss factor η (indicative of dissipated energy)

$$\eta = C\frac{\Delta\omega}{\omega_r} \tag{15}$$

where $C=1/\sqrt{n^2-1}$ and ω_r is the resonant frequency. For our case (half-power point), $n=\sqrt{2}$, and

$$\eta = \frac{\Delta\omega}{\omega_r}. \tag{16}$$

The mathematical model described previously estimates the unconstrained behavior very well, and we have calculated the fundamental frequency based on this model to be having the same order of magnitude. For the constrained treatment case, it is difficult to obtain the system parameters in closed form due to the presence of shear deformation, and hence, we have tried to model such cases using COMSOL MultiPhysics (version 4.1) and compared with the experimental data.

II. Experimental

A. Fabrication of the Microstructured Vibration Damper Slabs

In order to make a microstructured viscoelastic (PDMS) laminate, we use a process of replication through desirably sized copper wires duly knit in a plastic box in an array format. The array is created in a plastic box (breadth $=51$ mm, thickness $=17$ mm, and length $=80$ mm) by drilling 200-μm diameter holes in a rowwise and columnar fashion with a center-to-center distance of 2 mm rowwise and 2 mm columnwise, using Integrated Multi-process Machine Tool DT 110 (Mikro-tools, Singapore) using CNC programming. The holes drilled are laid out face to face on opposite walls of the box. Furthermore, copper wires with a diameter of 80 μm are inserted using special tweezers, bridging the gap between these holes on opposite faces, and the assembly is tightened on an in-house designed and developed fixture, as shown in Fig. 2(b). Here, we have used an 80-μm wire because of the following two reasons. First, its strength is high so that the replication of the microchannel can be complete and the wiremold can be taken out without breakage. Second, the diameter is large enough for a complete filling of the microchannel with silicone oil. If we use a lesser diameter of the wire, then due to wire breakage during the replication process, we are unable to formulate 100% through channels, and some of them get blocked. Thus, the complete array of microchannels seems to be utilized for vibration damping when the diameter is 80 μm. The wires are tightened longitudinally on the fixture using tightener pins. Replication of the slab is then performed using this architecture. PDMS prepolymer and its curing agent premixed in a ratio of 10 : 1 are poured in this mold and degassed in a desiccator, following which a curing step is proceeded in an oven maintained at 85 °C for 45 min. The fixture stands over a tripod arrangement, and leveling is performed prior to pouring the liquid PDMS. The polymer mix solidifies and entraps the copper wires, and this assembly is released carefully from the fixture and also the plastic housing. The hole diameter is slightly bigger than 80 μm, and this ensures that the wire is loosely inserted in the plastic box and thus easy to get removed with the embedding PDMS slab from the plastic box. This results in a slab with dangling copper wires across both ends, which is further swelled by immersing in toluene for 24 h. The toluene swells the PDMS matrix and loses the grip on the copper wires, which can then be taken out with the help of tweezers. The polymer is then subsequently deswelled by keeping it at room temperature for two days or in an oven maintained at 85 °C for 3 h. The hole center of the top row array is around 3 mm from the top surface of the final PDMS slab. Each row has 20 microchannels. Once the structured slab is ready, silicone oil is filled partially in the microchannels in a controlled manner with the help of a 1-ml syringe while the meniscus is observed with a magnifying glass. The injection of oil is made up to the point when the oil bead starts to formulate on the other end of the channel, indicating complete filling. We use silicone oil as it can be filled easily without substantial modification of the overall mass of the damper. The characteristic properties of silicone oil are density $=960-1050$ kg/m^3 and viscosity of 950–1050 cSt. Vibrational energy is dissipated because of the shear between

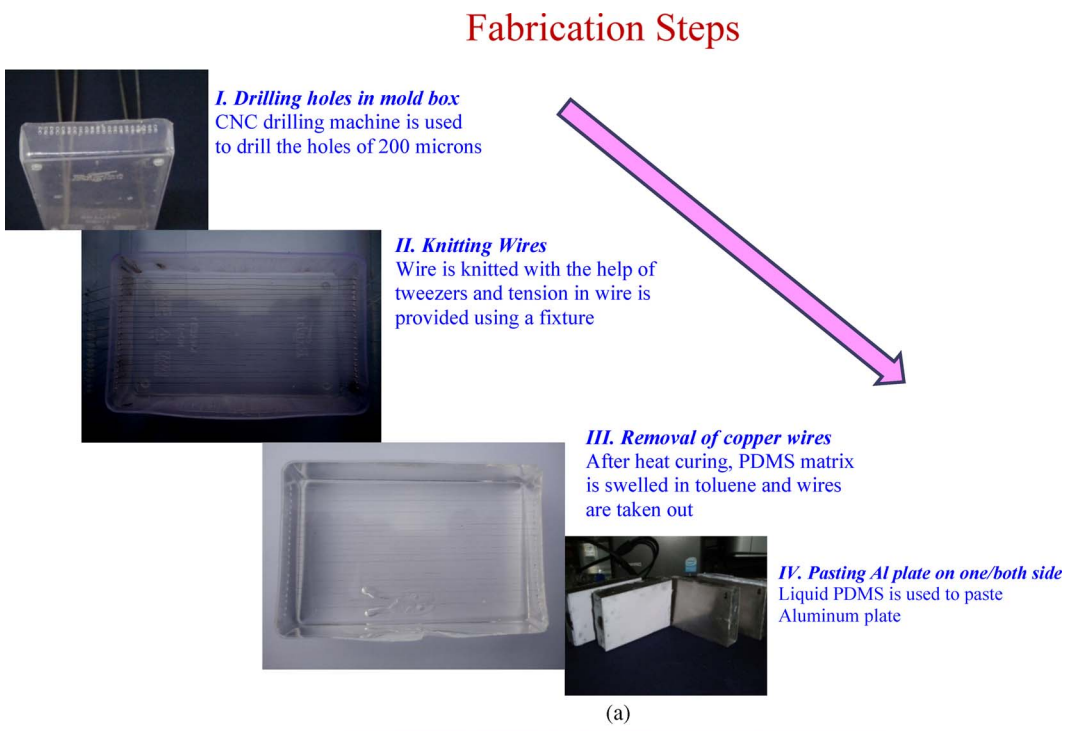

Fig. 2. (a) Different steps of fabrication of the damper assembly. (I) Drilling holes in the plastic mold. (II) Inserting the wire array and using the fixture to provide longitudinal tension for consistency of the microchannels and replication with PDMS. (III) Removal of the molding wires to obtain a straight array of microchannels. (IV) Pasting the aluminum plates at the bottom for unconstrained damping and at both top and bottom for constrained damping. (b) Tensioner fixture for tightening the replicating wires to ensure straightness of the features.

TABLE I
GEOMETRIC DETAILS OF THE MICRODAMPER ASSEMBLY (SIX ROWS OF MICROCHANNELS—CONSTRAINED TREATMENT)

Micro-damper Elements/Axis Dimension/Position	
Aluminum Plate (Base plate & constraining plate)	81×50×1.46 mm
Distance of central axis of top rows of micro-channels from top surface of PDMS layer	3 mm
Distance between central axes of first, second, third and fourth row	2 mm
Diameter of micro-channels	80 micron
Length of micro-channels	61 mm
Plug length (Both side)	10 mm
Distance of central axis of first channel of all rows from sidewall	6 mm

the layers of the confined oil volume within the microchannels and also because of the frictional dissipation due to the relative movement of the confined oil within the PDMS. The lengths of the slab and the embedded microchannels are both 81 mm. In order to plug the injected oil filled in the microchannels, both ends (along the channel length) of the slab are cut using a sharp cutter, this slab (shorter length) is placed upside down and centered in another new box (without any drilled holes), and liquid PDMS mix is filled on both cut ends and then heat cured. PDMS on curing gets cross-bonded and becomes an integral part of the slab, thus plugging and enclosing the filled up oil. In this way, the microchannels are plugged so that oil

does not come out. The oil moves within the channel as the PDMS flexes, and the channels deform, causing movement of oil within their various sections so that the continuity can be maintained. Also, in this way, there is control on the positioning of the microchannel array from the top of the slab as there is no level difference on the lower side of the slab. The level difference on the opposite side of the slab (facing up in the box) is controlled by metering the liquid PDMS in a manner so that it just rides over the top surface of the slab. On curing, the whole liquid becomes an integral part of the slab. The slab is further pasted to a well-milled aluminum base plate of the size of the slab and with a thickness of 1.46 mm by using the PDMS mix (PDMS prepolymer and its curing agent) and then again curing the assembly for the unconstrained treatment. In the constrained treatment, the only difference is that a similar aluminum plate is pasted on the top side of the assembly, sandwiching the microstructured slab between this and the base plate. Fig. 2(a) shows the fabrication flowchart with some photographs of the various steps. Fig. 2(b) shows a photograph of the wire tensioner used to replicate the microchannels. Microchannel rows 1–6 were fabricated in different PDMS blocks by the aforementioned method for the dampers. In one case, the equivalent volume of the microchannels corresponding to the maximum row case (six rows) was carved in PDMS as two large channels at the geometrically centered plane of the block with equal internal spacing. This was performed to gauge the efficacy of microstructuring over macroscopic features and structures. This is referred to as macroscale equivalent of six rows (MESR).

B. Simulation Details

The eigenfrequencies for all samples of unconstrained and constrained treatment cases have been solved using COMSOL MultiPhysics (version 4.1; simulation tool). All simulations have been performed using a business PC with 16-GB RAM and Intel (R) Core (TM) i7 CPU @ 3.07 GHz running on 64-b Windows 7 Professional operating system.

The microdamper geometries have been created according to Table I and have been meshed with normal mesh type. The mesh size and density get self-regulated upon approaching a channel cavity or a corner. Mesh optimization was done by running the simulation on different mesh densities. The parameters evaluated were z-displacement of the geometric center of the top surface of the damper assembly. The simulation was performed with "both ends fixed configuration." While doing simulations, the aluminum plate, PDMS layer, and silicone-oil-filled microchannels have been assigned linear elastic material model, viscoelastic material model, and hyperelastic material model as required by the material properties. The silicone-oil-filled microchannels were modeled as hyperelastic material to accommodate high strain values. Young's modulus of aluminum as confirmed by tensile tests run on UTM comes out as 53.51 GPa, and this value has been used for all of the calculations as well as simulations. The degradation of the tensile strength of the metal plate from around 70 GPa as in the case of pure aluminum is probably because of alloying and impurities. We assume zero displacement and velocity at time $t = 0$. The microdamper was modeled using solid mechanics module, and the eigenfrequencies were determined.

TABLE II
INPUT MATERIAL PROPERTIES FOR THE COMSOL MULTIPHYSICS SIMULATION

Aluminum		
	Young's modulus	53.51×10^9 Pa
	Density	2063.95 Kg/m^3
	Poisson's ratio	0.35
PDMS		
	Bulk modulus	0.962×10^6 Pa
	Shear modulus	250×10^3 Pa
	Density	970 Kg/m^3
Silicone Oil		
	Density	980 Kg/m^3
	Lame Constant, μ	1.43×10^9 Pa
	Lame Constant, λ	1×10^{10}~1×10^{16} Pa

Supplementary Information

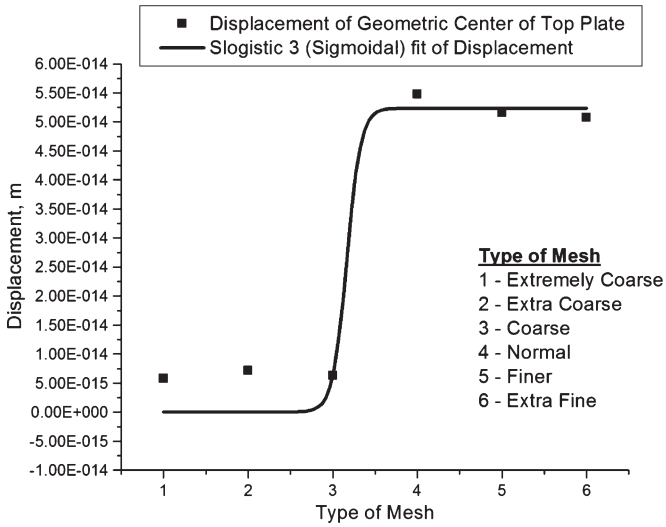

Fig. S1. Mesh optimization plot with the target parameter of amplitude displacement for the four-channel case. The plot shows consistency in reported displacement amplitudes for normal, finer, and extrafine meshes.

The following are the governing equations executed by the solver:

$$-\rho\omega^2 - \nabla.\sigma = F_v$$
$$-i\omega = \lambda$$

where ρ, ω, σ, λ, and F_v are density, angular frequency, stress, eigenvalue variable, and excitation force, respectively. We have presented the simulations of microdamper for constrained and unconstrained treatment cases from one row of microchannel up to six rows of microchannels by calculating the fundamental frequency. Simulations are also done on the MESR case. The simulation software also computes the vertical displacement of the surface of microdamper and shows along with the fundamental mode frequency. The input parameters that were used in generating the simulation are illustrated in Table II. The simulation also computes the strain energy at every point of the microdamper. The mesh optimization was also done, and the same is shown in supplementary Fig. S1. The number of elements for various mesh types is given in supplementary Table S1.

TABLE S1
NUMBER OF ELEMENTS FOR VARIOUS MESH TYPES

Type of Mesh	Max & Min element size	No. of elements	No. of degrees of freedom solved for
Extremely coarse	0.0305/0.0043 m	38716	329910
Extra Coarse	0.0183/0.00329 m	77683	647073
Coarse	0.00915/0.00171 m	140964	1251051
Normal	0.0061/0.0011 m	177084	1566624
Finer	0.00335/2.44e-4	266571	2273265
Extra Fine	0.00213/1.26e-5 m	430865	3387210

C. Experimental Setup for Vibration Measurements

The experimental setup for investigating the vibration suppression qualities of the microstructured damper (realized earlier) is based on the study of the transmissibility of an excitation signal by scanning the damper surface with a single-point laser detector. The damper is mounted with both ends fixed in a simply supported beam configuration. The ends are clamped using a knife edge support on both ends which overlaps about 10 mm on both sides of the damper to provide a firm grip. The excitation signal is applied from the geometric center on the bottom surface of the aluminum base plate on the damper assembly by means of a shaker (model V201, LDS, Germany). The direction of the excitation signal used was vertical. Longitudinal damping is mostly investigated in high-frequency vibrations. The transverse or vertical damping is investigated for low-frequency vibrations. Longitudinal damping is a phenomenon of mass-dominated damping. It means that, if fluid heavier than silicone oil or PDMS is used, then an analysis of longitudinal damping would be necessary. As we are using silicone oil (the density is the same as PDMS) in the channels, the overall change of mass is insignificant; although there is an overall stiffness change, the oil confined within the microchannels increases the stiffness of the structure. Thus, it is appropriate to investigate the transverse damping behavior of our system, which is performed by coupling the shaker to the damper assembly as illustrated previously. The shaker is connected to an amplifier (model PA 25E, LDS, Germany) and a function generator (model ST 4060, ScienTECH, India) which applied a sinusoidal signal (1.5 V peak to peak) and an amplifier gain of 2. The excitation is provided over a range of frequency values by manually varying the output of the signal generator from 0 to 1000 Hz in steps of 1 Hz, which can be read on the screen of the generator. We scan the top surface of the damper by recording the displacement of its geometric center by a single-point laser sensor (model OptoNCDT 1700, MICRO-EPSILON, Germany). The recorded data are acquired by a software ILD 1700 Tool V2.31.

When the external signal matches with the natural frequency of vibration of the damper slab, there are large amplitudes of motion due to resonance, and this point is identified by means of an increased humming sound (the vibrating beam produces a series of compression and rarefaction in air). The frequency corresponding to this point is recorded from the signal generator's screen and is the fundamental mode frequency. This is also shown by surface displacement (top) of microdamper by single-point laser, as shown by supplementary Fig. S2. Fig. 3 shows a schematic of the setup. We also record the vibration suppression

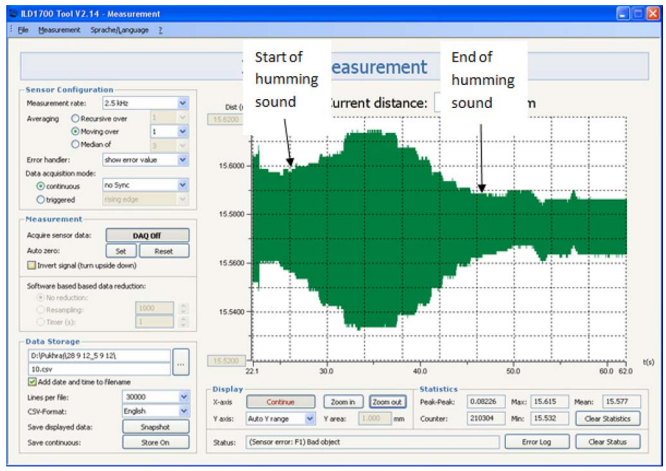

Fig. S2. Snapshot of the computer screen connected to a single-point laser sensor.

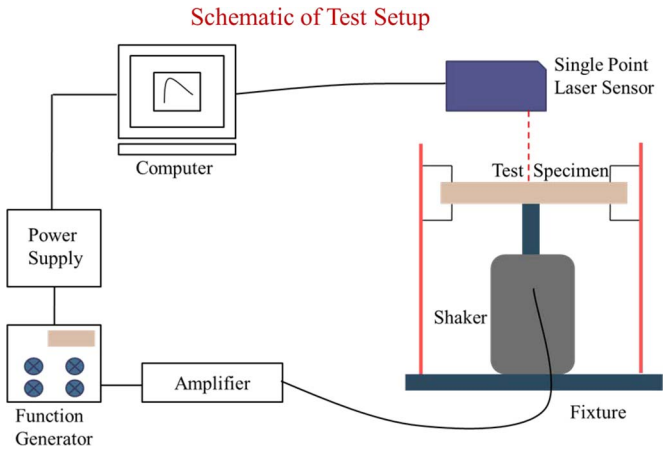

Fig. 3. Schematic of the test setup for measurement of the fundamental mode frequency with a shaker table connected to a feeding function generator (range 0–1070 Hz), an amplifier (model PA 25E, LDS), and a power supply, and a single-point laser sensor (model OptoNCDT 1700, MICRO-EPSILON) connected to a computer interface for real-time data acquisition.

of the damper slab by providing it an impact through a hard hammer on the aluminum base plate of the assembly and record the amplitude of displacement of the top surface temporally using the single-point laser scanner described earlier and subsequently plotted using Origin 8. We have observed a difference in the time taken by the damper for suppressing this impact as we modify the damper structurally. We further analyze the data and find out the logarithmic decrement of amplitude from this plot from which we get the damping ratio (the details are in the theoretical section).

TABLE III
FUNDAMENTAL MODE FREQUENCY VALUES FOR UNCONSTRAINED AND CONSTRAINED CASES OBTAINED THROUGH SIMULATION AND EXPERIMENTAL METHOD

No. of rows of Micro-channels in sample[a]	Simulation		Experimental	
	Unconstrained Treatment	Constrained Treatment	Unconstrained Treatment	Constrained Treatment
Without Channel	288.1 Hz	337.9 Hz	272 Hz	348 Hz
One	304.7 Hz	388.3 Hz	290 Hz	351 Hz
Two	490.9 Hz	580.1 Hz	494 Hz	578 Hz
Three	512.6 Hz	596.6 Hz	511 Hz	602 Hz
Four	514.8 Hz	601.2 Hz	518 Hz	606 Hz
Five	515.7 Hz	605.9 Hz	522 Hz	611 Hz
Six	526.7 Hz	632.9 Hz	529 Hz	617 Hz
MESR	290.5 Hz	350.9 Hz	275 Hz	391 Hz

[a]No. ofmicro-channels in each row = 20 , MESR – Macro scale equivalent of six rows

D. Particle Image Velocimetry

In order to see the flow behavior of the enclosed fluid within the microchannel (coupled with the external vibrational energy), a platform is realized in PDMS containing a microchannel with a width of 200 μm and a depth of 40 μm. This microchannel is plasma bonded to a hard glass substrate which is imaged from the top side by the $10\times$ objective of a fluorescence microscope (NIKON Eclipse 80i). The microchannel structure is made hydrophilic by treating with polyethylene glycol [19] and is then filled with a water solution of fluorescently labeled polymer microbeads with a size of 1 μm (concentration of 0.05% by volume). After filling this solution, the inlet and outlet ports of this microchannel are closed by silicone sealant (Silastic 732 RTV, Dow Corning India Pvt. Ltd., Pune, India). The microchannel is coupled with the mechanical vibrations coming out of a shaker connected to an amplifier and a function generator supplying a sinusoidal input. The excitation frequency and amplifier gain used were 7 Hz and 1.2, respectively. The CCD camera mounted on the microscope recorded snapshots at an interval of 0.100 s using the Image Pro Express 6.0 software. These snapshots were further analyzed using Dynamic Studio version 1.45 (Dantec Dynamics Inc.) software to find out the velocity vector plots.

III. RESULT AND DISCUSSION

A. COMSOL MultiPhysics (Version 4.1) Simulations

The fundamental mode frequency as obtained from simulation is shown in Table III and also Fig. 4 (by the hatched bars) for both constrained and unconstrained treatments. The mesh optimization has been done on maximum mesh sizes varying between 0.0305 m (for the extremely coarse mesh) and 0.00213 m (for the extrafine mesh). It may be noted that, for a certain mesh density, the meshing is self-regulated upon approaching a crevice, corner, or cavity (microchannels). Thus, as normal mesh is used, the mesh sizes may vary from a maximum of 0.00213 m to 12 μm throughout the block volume. The parameter for optimization was taken as the z-displacement of the geometric center of the damper assembly's top surface, and the optimized mesh size obtained corresponds to 0.0061 m (see supplementary Table S1). We assume that the z-displacement is the most critical parameter in our experiments for the calculation of the damping ratio and the fundamental frequency should be the target parameter for optimization.

All simulations therefore are performed using normal mesh size. We observe an increase in fundamental mode frequency with increasing number of microchannel rows from 304.7 Hz (corresponding to one row) to 526.7 Hz (corresponding to six rows) for the unconstrained damping and an identical behavior in case of constrained damping. The frequency in the constrained case varies from 388.3 to 632.9 Hz. The overall increase in the fundamental mode frequency from the unconstrained to constrained case can be attributed to an increase in the flexural rigidity of the constrained configuration because of an additional aluminum plate sandwiching the damper assembly (refer to (11), assuming a constant frequency parameter for all of our experiments [17]).

The increase of the fundamental mode frequency in the unconstrained case is 72.9% as the number of microchannel rows is varied from one to six. This increase for the constrained case is similar (around 62.9%). Therefore, the variation in the frequency by adding more number of rows of microchannels can be attributed to the fact that the stiffness of the viscoelastic slab increases as more rows of oil-filled and plugged microchannels are added. Stiffness is proportional to the square of the fundamental mode frequency $[f = (1/2\pi)\sqrt{k/m}]$. As the volume density of the silicone oil (980 Kg/m^3) used to plug the microchannels is slightly above that of the PDMS material (970 Kg/m^3), the increase in overall mass of the damper due to the addition of rows is quite compensated by the increase in rigidity due to the addition of the first set of rows. However, as additional rows are added, the stiffness increases significantly in comparison to the increase of mass. Thus, the frequency suddenly increases from 304.7 to 490.9 Hz in the unconstrained case and from 388.3 to 580.1 Hz in the constrained case as the number of rows is increased from one to two. After this, any additional increase in the number of rows results in an increase in fundamental mode frequency primarily attributing to the enhancement of volume stiffness. We found out from our simulation results that there are hardly any deflections in both rigid aluminum plates, and the slice plot shows a huge nonuniform deformation of the viscoelastic damping layer, which is quite in line with any sandwich layer of a damping

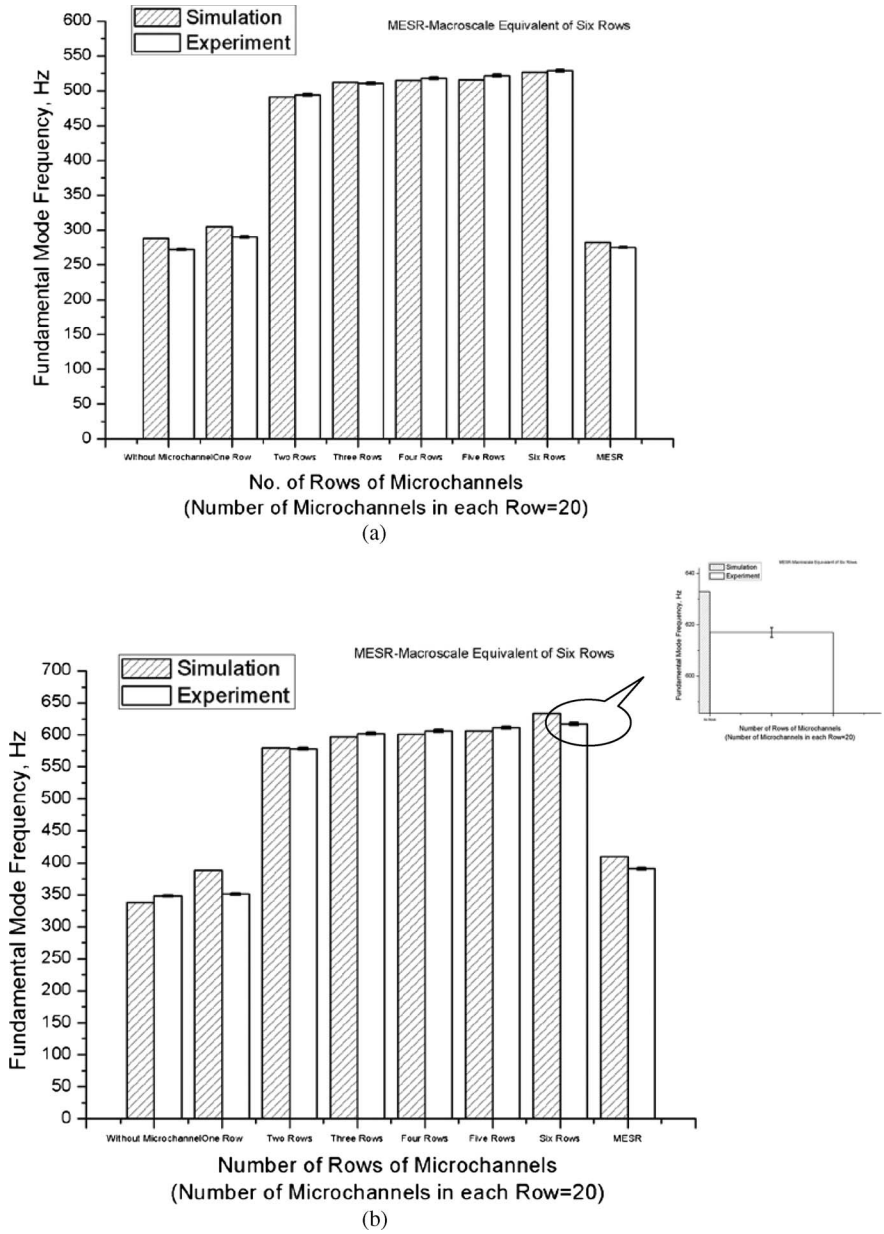

Fig. 4. Fundamental mode frequency versus the number of rows of microchannels, indicating the frequency bars for cases with no channel (with the number of channel rows as one to six and the MESR case). (a) For unconstrained treatment. (b) For constrained treatment.

arrangement. Maximum deformation is observed in this layer and accounts for the dissipation of vibrational energy by friction heating. In the MESR case, the simulated frequency comes out as 290.5 Hz in the unconstrained case and 350.9 Hz in the constrained treatment. Thus, the MESR block frequency is higher than the "no channel" case but lower than the "single row" case. This indicates that the stiffness-to-mass ratio of the blocks increases as microchannels are distributed throughout the bulk. If an equivalent volume is carved out in a manner concentrated at a few regions, the stiffness-to-mass ratio does not show much increase.

The experimental analysis shows a similar trend in the fundamental mode frequency as detailed later. We have also observed experimentally that the damping ratio of these microvibration dampers increases with an increase in the number of rows of channel layers. In order to explain this behavior, we performed simulations for predicting the strain energy per unit volume. The strain energy per unit volume data were extracted from the oil filled in the microchannel region (along the axis of the

TABLE IV
COMSOL MULTIPHYSICS SIMULATION—STRAIN ENERGY PER UNIT VOLUME (IN JOULES PER CUBIC METER) AT 20 mm OF MIDDLE CHANNEL IN FIRST ROWS OF FOUR ROWS OF MICROCHANNELS OF THE CONSTRAINED TREATMENT CASE

Position	Strain energy per unit volume (J/m^3)
40 micron depth from wall in PDMS	-2376
Wall of the micro-channel	-7.29×10^4
Along the axial center of the micro-channel	-4935

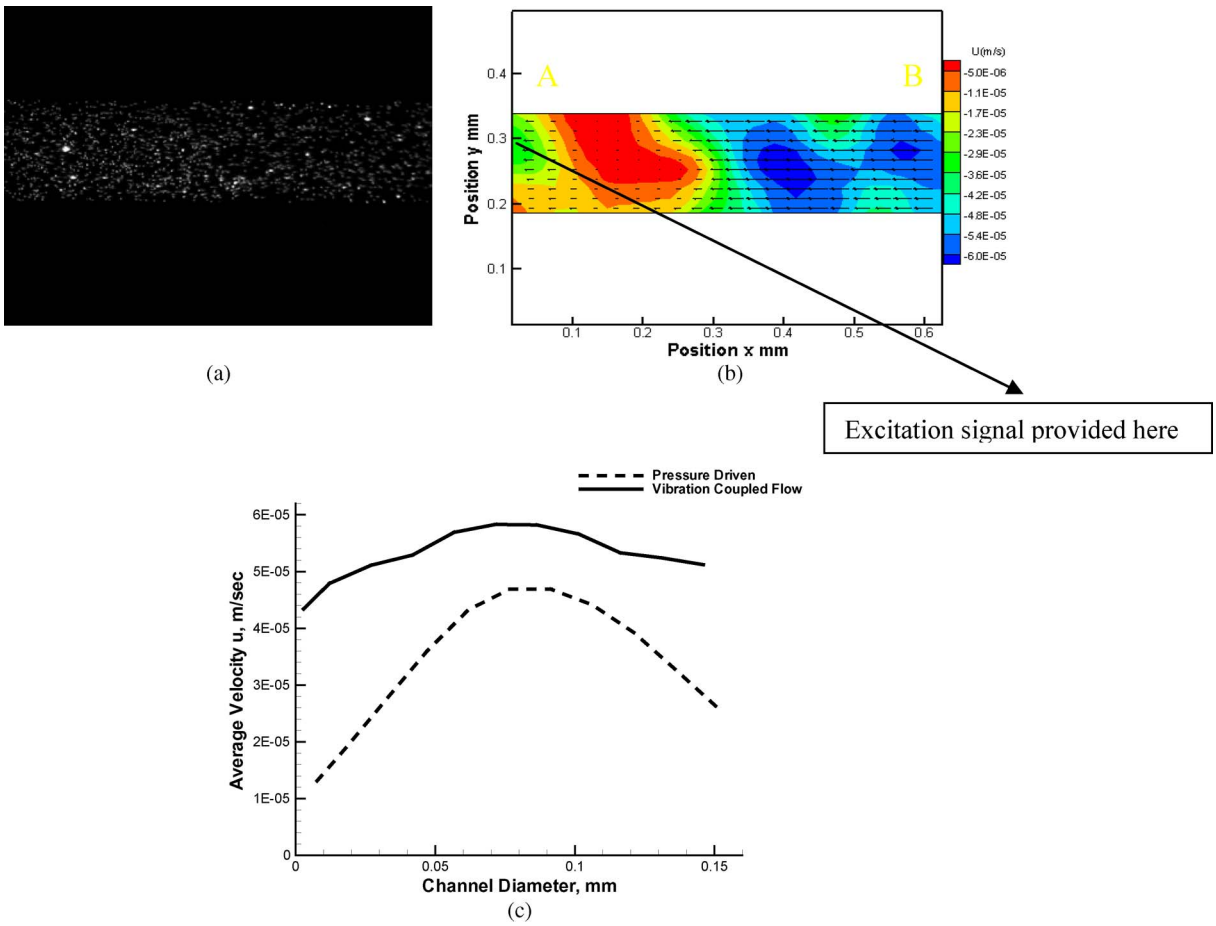

Fig. 5. (a) Microchannel image using an optical magnification of $10\times$ with microbeads (fluorescently labeled) in motion that are inserted inside the damper block with a single representative channel filled up. (b) Contour plot of velocity vectors, using Dynamic Studio analysis software, possessed by the moving microbeads on coupling of vibrational energy to the damper block (the velocities are time averaged on the basis of 10 frames/s speed of acquisition. (c) Comparison of velocity profile in the radial direction between pressure driven flow and vibration coupled flow, indicating a slip boundary condition with a negligible velocity reduction in case of the solid lines for vibration coupled flow.

microchannel), the polymer layer close to the microchannel surface (at a depth of 40 μm), and the channel wall. All data were extracted at a length of 20 mm from the end of the microchannel (Table IV). The energy dissipation is represented by negative strain energy, with the highest dissipation at the interface of the oil and the PDMS channels $(-7.29 \times 10^4$ J/m$^3)$. We have separately studied the fluid structure interaction model to find out a suitable reason for this extremely high energy dissipation at the interface. As the microdamper is subjected to mechanical vibrations, the oil inside the microchannels creates a slip condition with the channel walls, and due to the friction generated at the oil–PDMS interface owing to the relative motion, the energy is dissipated. In other words, we could observe finite velocities of the fluid very near to the channel wall, and this shows a slip boundary at the channel walls. We hypothesize that this slip boundary comes from the bending and deforming of the channel, thus squeezing out the fluid containment of the silicone oil. Fig. 5(a) and (b) shows the microchannel image with microbeads in motion and the contour plot of the average bead velocity of a completely filled microchannel coupled with vibration energy. In this plot, region "A," which is very near the excitation source, has a negligible average velocity due to very less available relaxation time for the microbeads between their bidirectional motions (which is caused by the squeezing and expansion of the microchannel as the excitation source is coupled to the structure). The particles which are far away from the source get more relaxation time and thus possess a higher average velocity (region "B"). Also, the average velocity is higher in the direction of suction created because of the post-squeezing expansion of the microchannel. We are able to see very clearly velocity vectors near the channel walls, suggesting a slip boundary condition. Fig. 5(c) shows a comparison of the average velocity profiles in the same microchannel in two different experiments, where, in one, a pressure driven flow is analyzed and, in the other experiment, a vibration coupled flow is analyzed by the use of Dynamic Studio. As can be clearly seen in the parabolic case represented by the dotted curve, the average velocity near the walls has almost an order of magnitude change, and in the vibration coupled case, the magnitude of the velocity remains almost the same at the center of the channel as well as the walls (as represented by the continuous curve). If the number of microchannels is increased, the energy dissipated on the channel surfaces is more, and thus, with the increase in the number of microchannels, the damping ratio increases. The same result is reflected with experimental studies.

B. Fundamental Mode Frequency: A Comparison Between Simulations and Experimentally Obtained Values

The experimental values for fundamental frequency as obtained at the point of resonance show a similar behavior with the theoretical values and simulation in the unconstrained case. These values are represented by open bars in Fig. 4(a) and (b). The fundamental mode frequency for the unconstrained case [Fig. 4(a)] as obtained experimentally varies from 290 to 529 Hz for cases 1–6 rows, respectively. The theoretical model estimates these values as 475.7–483.67 Hz, but the simulations estimate these values from 304.7 to 526.7 Hz. The theoretically obtained values do not show much variation with varying number of microchannels but do report the fundamental frequency within the same order of magnitude. The theoretical model in our opinion would need further fine tuning, which will be included in a future endeavor. The numerical calculations, experimental analysis, and simulations are repeated for the no channel case and the MESR for a comparison. Simultaneously through simulations and experiments, this value is reported as 288.1 Hz (lower than the one-row case) and 272 Hz, respectively. For the MESR, these values (i.e., through simulations and experiments) come out as 290.5 and 275.0 Hz. Therefore, in this case as well, the MESR value comes in between the no channel and one-row cases for reasons indicated earlier. The experimental values are in close proximity to the simulation results, which is not true for the analytically predicted values. A similar behavior is observed in the constrained case [Fig. 4(b)], where the fundamental mode frequencies are estimated with simulations and compared with experiments. For the no channel case, the fundamental mode frequency is observed experimentally as 348.0 Hz and through simulations as 337.9 Hz. The frequency for the MESR is experimentally determined as 391 Hz and through simulation as 350.9 Hz. For the remaining case 1–6 rows, the values obtained through experimentation are 351–617 Hz, and through simulations, this is observed as 388.3–632.9 Hz. This demonstrates that the microstructured dampers exhibit a higher frequency bandwidth with microstructuring, which has never been reported earlier by some of the other researchers who studied the effects of damping and natural frequency by incorporating micro-/macroscale inclusions in viscoelastic materials. Therefore, most certainly for high-frequency damping applications, the use of such a technique is quite beneficial.

C. Damping Ratio and Loss Factor: COMSOL MultiPhysics Simulations and Experimental Findings

The damping ratio for the unconstrained and constrained treatment cases is calculated by the logarithmic decrement method as detailed earlier, wherein x_0 and x_n are from the time-displacement plot of the vibrating damper assembly. The damping ratio is seen to be increasing with more number of microchannel rows (Fig. 6). The reason for this is as follows. When a microdamper is subjected to vibration, the oil inside the microchannels moves in it. We have already shown through fluid structure interactions that the fluid movement along the channel walls results in a substantial amount of dissipation of vibration energy. As the number of channels is increased,

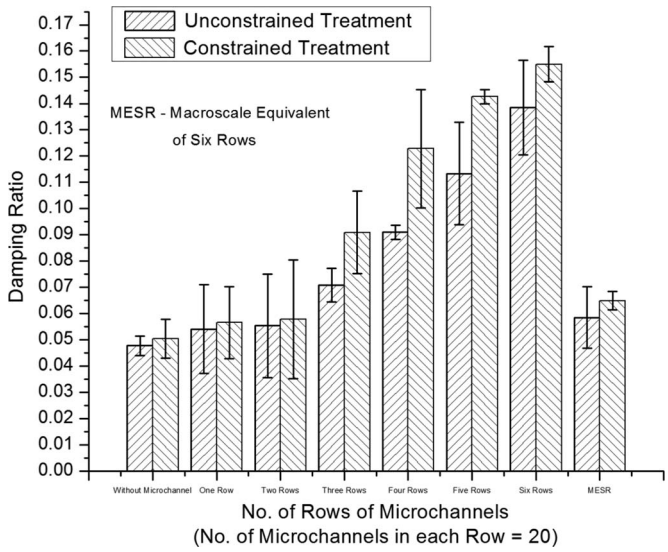

Fig. 6. Damping ratio in the unconstrained and constrained treatment cases for the block with no microchannels and with microchannel rows varying from one to six and the MESR case.

this interfacial area with the silicone oil also increases, resulting in more frictional dissipation. For the unconstrained case, the damping ratio varies from 0.055 to 0.14 (2.7 times increase), whereas for the constrained case, this is recorded to vary between 0.056 and 0.16 (2.8 times increase) as the rows vary from one to six. These values are almost double that of earlier reported literature [12] on room temperature damping using microscale inclusions in viscoelastic materials. The damping ratio for the constrained treatment cases is more than the unconstrained treatment case for all corresponding samples. This can be attributed to the contribution coming from the shear deformation initiated by the top plate. As per (11), the fundamental mode frequency is proportional to the square root of rigidity if the other parameter remains constant. The equivalent thickness is dependent on the thickness of the layers used. The rigidity is proportional to the equivalent thickness of the layers used. For the same configuration, the equivalent thickness of the constrained treatment mode is more than that for the unconstrained treatment mode. In this way, we can say that, due to more rigidity, the damping capacity of the microdamper is more in case of constrained treatment.

The loss factors of the constrained and unconstrained cases are calculated by using the half-power bandwidth method. Fig. 7(a) shows the amplitude versus normalized frequency ($\Omega = \omega - \omega_r$, where ω_r is the fundamental mode frequency) representative plots for one (solid line), three (dashes), and five (dotted line) channel cases on experimentally acquired amplitude–frequency data. The plot clearly illustrates a decreasing sharpness corresponding to increasing bandwidth and a reduction in the overall displacement amplitude for all of these cases as the number of rows is increased. The reduction in displacement amplitude further indicates the energy dissipative behavior of the system. Fig. 7(b) shows the calculated loss factor from this half-power bandwidth curve for both unconstrained and constrained cases, respectively. The loss factor of the unconstrained case varies from 0.02 to 0.11 (about 5.5 times increase), and in the constrained case, it varies from 0.019 to

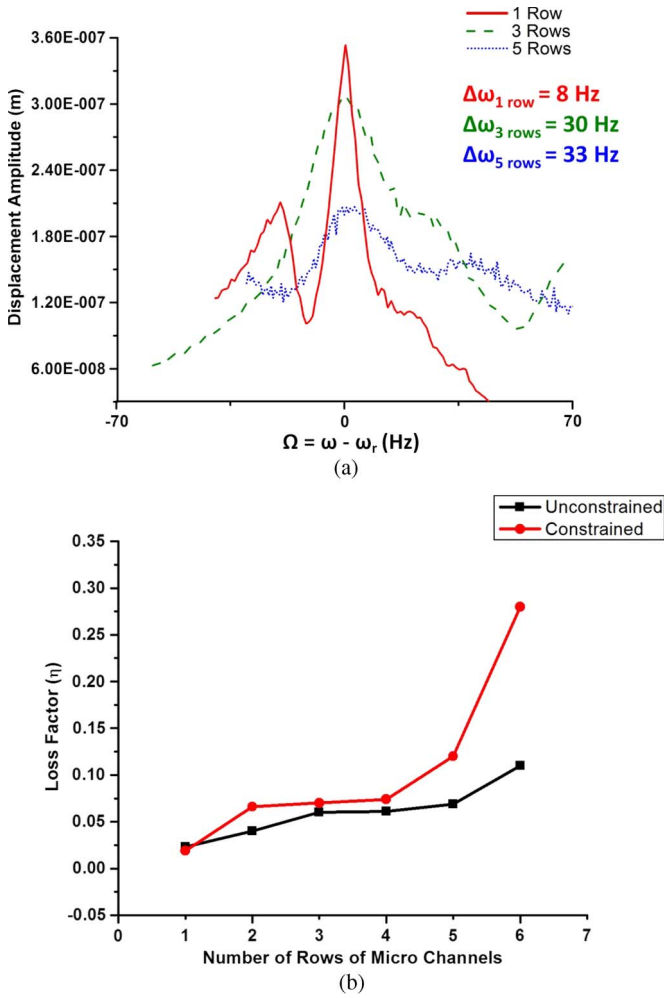

Fig. 7. (a) Plot of displacement amplitude versus half-power bandwidth in case of a representative sample of one, three, and five rows for the unconstrained treatment case. (b) Plot of calculated loss factor for the number of channel rows of one to six and MESR cases.

0.28 (about 14.7 times increase) for the one- to six-row cases, respectively. This increase in loss factor is indicative of a higher energy dissipation in the constrained case for similar reasons as in the case of the damping ratio. Also, worth noting is the fact that the loss factor for the constrained case has an order of magnitude increase with the increase in number of channel rows and compares reasonably with earlier reported work of Kaully *et al.* [13], although in our case, the operating temperature is room temperature throughout the experiments.

This energy dissipative behavior explored in the aforementioned experiments shows a good promise because of high damping ratio and loss factor which is observed mostly at room temperature. In the process of energy dissipation, there is an overall increase in the temperature of the damper, but the properties of the material remain unchanged due to this temperature rise as the damper shows identical behavior in successive runs.

IV. Conclusion

We have developed a novel custom-made damping pad with different damping ratios and fundamental frequencies using a microstructuring technique. As we have discussed, by virtue of adding more number of rows of microchannels in the PDMS damping slab, we can suitably vary its damping properties. We have further found out a relationship between the fundamental frequency for two different test cases of constrained and unconstrained treatment and number of microchannel layers or rows. Damping ratios can be changed from 0.056 to 0.16 (around 3 times), and fundamental mode frequency can be increased from 288 to 617 Hz by virtue of this microstructuring. We have also observed a high energy dissipation at the interface of the microchannels and the oil containment within them, and this results from the creation of a slip zone causing frictional dissipation of energy. While the current study has shown that high damping is achievable using microscale channels, the nature of damping with respect to the change in vibration amplitude per cycle will be studied in the future to find the linearity of the damping phenomena. The approach demonstrated in this paper will open a future domain for customized damping arrangements and would find a lot of applications in electronic devices and systems, automobile seating system, etc., which may need custom-made vibration suppression mechanisms at a variety of operational frequencies.

Acknowledgment

The authors would like to thank the Center for Nanosciences, Indian Institute of Technology, Kanpur, India, and Prof. S. Gangopadhyay, Prof. K. Gangopadhyay, and A. Ghosh of the University of Missouri, Columbia, MO, USA, for their help, advice, and valuable suggestions. The authors would also like to gratefully acknowledge the help rendered by S. Varanasi in the experimental work.

References

[1] B. Bhattacharya, J. A. Rongong, and G. R. Tomlinson, "Vibration suppression performance of piezoceramic and magnetostrictive materials in hybrid constrained layer damping," in *Proc. SPIE*, 1999, vol. 3672, pp. 242–250.

[2] C. W. D. Silva, *Vibration Fundamentals and Practice*. Boca Raton, FL, USA: Taylor & Francis, 2007.

[3] A. K. Mallik, *Principles of Vibration Control*. New Delhi, India: Affiliated East West Press Pvt. Ltd., 2010.

[4] B. Bhattacharya, G. R. Tomlinson, and J. R. House, "Vibration suppression of structures with viscoelastic inserts," *Proc. Inst. Mech. Eng., J. Mech. Eng. Sci.*, vol. 216, pt. 10, pp. 983–995, Oct. 2002.

[5] T.-L. Teng and N.-K. Hu, "Analysis of damping characteristics for viscoelastic laminated beams," *Comput. Methods Appl. Mech. Eng.*, vol. 190, no. 29, pp. 3881–3892, Apr. 2001.

[6] E. M. Kervin, "Damping of flexural waves by a constrained viscoelastic layer," *J. Acoust. Soc. Amer.*, vol. 31, no. 7, pp. 952–962, 1959.

[7] D. Ross, E. E. Unger, and E. M. Kervin, Jr., "Damping of plate flexural vibrations by means of viscoelastic laminates," in *Proc. ASME Struct. Damping ASME*, New York, NY, USA, 1959, pp. 49–88.

[8] Y. V. K. S. Rao and B. C. Nakra, "Vibrations of unsymmetrical sandwich beam and plates with viscoelastic cores," *J. Sound Vibrat.*, vol. 34, no. 3, pp. 309–326, 1974.

[9] C. D. Johnson, "Design of passive damping systems," *J. Mech. Des.*, vol. 117, no. B, pp. 171–176, Jun. 1995.

[10] J. L. Marcelin, S. Shakhesi, and F. Pourroy, "Optimal constrained layer damping of beams: Experimental and numerical studies," *Shock Vibrat.*, vol. 2, no. 6, pp. 445–450, 1995.

[11] R. K. Patel, B. Bhattacharya, and S. Basu, "A finite element based investigation of obtaining high material damping over a large frequency range in viscoelastic composite," *J. Sound Vibrat.*, vol. 303, no. 3–5, pp. 753–766, 2007.

[12] A. Goel, A. Kumar, P. K. Patra, S. Mahendra, S. Tabatabaei, P. J. J. Alvarez, G. John, and P. M. Ajayan, "*In situ* synthesis of metal nanoparticle embedded free standing multifunctional PDMS films," *J. Macromolecular Rapid Commun.*, vol. 30, no. 13, pp. 1116–1122, 2009.
[13] T. Kaully, A. Siegmann, and D. Shacham, "Mechanical behavior of highly filled natural $CaCO_3$ composites: Effect of particle size distribution and interface reactions," *J. Polymer Composites*, vol. 29, no. 4, pp. 396–408, Apr. 2008.
[14] Q. Wang, F. Han, and C. Cui, "Effects of macroscopic graphite particulates on the damping behaviour of CuAlMn shape memory alloy," *J. Mater. Sci.*, vol. 42, no. 13, pp. 5029–5035, Jul. 2007.
[15] A. Kocabas and A. Atilla, "Polymeric waveguide Bragg grating filter using soft lithography," *Opt. Exp.*, vol. 14, no. 22, pp. 10 228–10 232, Oct. 2006.
[16] M. Meyers and K. Chawla, *Mechanical Behaviour of Materials*, 2nd ed. Cambridge, U.K.: Cambridge Univ. Press, 2009.
[17] A. W. Leissa, "The free vibration of rectangular plates," *J. Sound Vibrat.*, vol. 31, no. 3, pp. 257–293, 1973.
[18] E. J. Hearn, *Mechanics of Materials*, vol. 1. Oxford, U.K.: Butterworth, 1997.
[19] P. B. Lillehoj and C.-M. Ho, "A long-term, stable hydrophilic poly(dimethylsiloxane) coating for capillary-based pump," in *Proc. IEEE 23rd Int. Conf. MEMS*, Sep. 4, 2011, pp. 1063–1066.

Rajeev Kumar Singh received the B.E. degree in mechanical engineering from Nagpur University, Nagpur, India, in 1992 and the M.Tech. degree in industrial systems engineering from Kamla Nehru Institute of Technology, Sultanpur, India, in 2007. He is currently working toward the Ph.D. degree in the Department of Mechanical Engineering, Indian Institute of Technology, Kanpur, India.

His research interests include MEMS, microfluidics, and microfabrication.

Rishi Kant received the B.Tech. degree in mechanical engineering from the University Institute of Engineering and Technology, Chhatrapati Shahu Ji Maharaj University, Kanpur, India, in 2004 and the M.E. degree in mechanical engineering from Delhi College of Engineering, University of Delhi, New Delhi, India, in 2007. He is currently working toward the Ph.D. degree in mechanical engineering at the Indian Institute of Technology, Kanpur.

He was a Research Assistant with the Design Manufacturing Integration (DFM) Laboratory, Indian Institute of Technology, New Delhi, from 2007 to 2008. His research interests include bio-MEMS and micro-/nanofabrication for fluidic and other applications.

Shashank Shekhar Pandey received the B.Tech. and M.Tech. degrees in mechanical engineering from the Indian Institute of Technology (IIT), Kanpur, India, in 2010. He is currently working toward the Ph.D. degree in bioengineering at the University of Utah, Salt Lake City, UT, USA.

He was with Daimler India Commercial Vehicles Pvt. Ltd. from 2010 to 2011. Thereafter, he was a Research Associate with the BioMEMS and Microfluidics Laboratory, IIT, from 2011 to 2012. His research interests include micro-/nanofabrication, biosensors, bioinstrumentation, bio-MEMS, microfluidics, and their applications in various engineering and medical problems.

Mohammed Asfer received the B.E. degree in mechanical engineering from Utkal University, Bhubaneswar, India, in 2003 and the M.Tech. degree from the Indian Institute of Technology, Kanpur, India, in 2007, where he is currently working toward the Ph.D. degree in mechanical engineering.

His research interests include development of microfluidic components (e.g., mixers, sensors, etc.) and simulation of microscale flows.

Bishakh Bhattacharya received the B.E. degree in civil engineering and the M.E. degree in applied mechanics from Jadavpur University, Kolkata, India, in 1988 and 1991, respectively, and the Ph.D. degree in aerospace engineering from the Indian Institute of Science, Bangalore, India, in 1997.

He subsequently carried out postdoctoral studies at the Department of Mechanical Engineering, Sheffield University, Sheffield, U.K., for more than two years. He joined the Department of Mechanical Engineering, Indian Institute of Technology, Kanpur, India, in 2000, where he is currently a Professor and the Head the Interdisciplinary School of Design. His research interests include smart materials and intelligent system design for varied engineering applications.

Pradipta K. Panigrahi received the B.Tech. (Honors) degree in mechanical engineering from UCE Burla, India, in 1987. He received the M.S. degree in mechanical engineering in 1993, the M.S. degree in system science in 1997, and the Ph.D. degree in mechanical engineering in 1997 from Louisiana State University, Baton Rouge, LA, USA.

He is a Professor with the Department of Mechanical Engineering, Indian Institute of Technology, Kanpur, India. His research focuses on development and implementation of various experimental techniques (primarily optical) for both macroscale and microscale applications to study both fundamental and practical aspects of a wide range of engineering systems.

Shantanu Bhattacharya received the B.S. degree in industrial and production engineering from the University of Delhi, New Delhi, India, in 1996, the M.S. degree in mechanical engineering from Texas Tech University, Lubbock, TX, USA, in 2003, and the Ph.D. degree in biological engineering from the University of Missouri, Columbia, MO, USA, in 2006.

He was a Senior Engineer with Suzuki Motors Corporation from 1996 to 2002. He also completed postdoctoral training at the Birck Nanotechnology Center, Purdue University, West Lafayette, IN, USA, for one year. He was an Assistant Professor with the Department of Mechanical Engineering, Indian Institute of Technology, Kanpur, India, from 2007 to 2012, where he is currently an Associate Professor. His research interests include design and development of microfluidics and MEMS platforms for varied engineering applications.